

On the Angular Resolution of Pair-Conversion γ -Ray Telescopes

D. Bernard,
LLR, Ecole Polytechnique, CNRS/IN2P3, 91128 Palaiseau, France

June 1, 2023

Proceedings of a presentation to Session 14, “Future spaceborne MeV detectors and related astrophysics”, of the 2023 International Conference of Deep Space Sciences, April 2023, Hefei, China

Abstract

I present a study of the several contributions to the single-photon angular resolution of pair telescopes in the MeV energy range. I examine some test cases, the presently active *Fermi* LAT, the “pure-silicon” projects ASTROGAM and AMEGO-X, and the emulsion-based project GRAINE.

keywords : γ -rays, pair production, telescope, angular resolution

1 Introduction

The *Fermi* Large Area Telescope (LAT) [1] has been watching the γ -ray sky for 15 years, has provided invaluable observations for over 6000 sources (12 years’ [2]), and is monitoring daily the full sky for transients possibly associated with gravitational wave detections or very high energy (VHE) neutrino detections, over a wide field of view (with an $\approx 2.5 \text{ m}^2 \text{sr}$ acceptance for an $\approx 1 \text{ m}^2$ effective area above 1 GeV [3]). None of us is eternal, though, and it is time to prepare for the γ -telescope of the next decade.

At lower energies, X-ray instruments such as the spectrometer SPI and the imager IBIS on Board the INTEGRAL Satellite [4], provide measurements with a similar sensitivity (Fig. 1). The situation is much less favorable, though, in the energy range 0.2 MeV – 0.4 GeV, that is, over three orders of magnitude, for which no instrument is available with a sensitivity lower (better) than $10^{-12} \text{ erg cm}^{-2} \text{ s}^{-1}$, while the last-century COMPTEL peaked above $10^{-10} \text{ erg cm}^{-2} \text{ s}^{-1}$. A consequence of the terrible limitation of the sensitivity of the available instruments is the terribly limited number of sources that can be studied in the MeV energy range (Fig. 2). A number of instruments are being developed though, so as to study the γ -ray sky in the future post-LAT era, and to fill the MeV sensitivity gap.

The so-called differential flux sensitivity, s , is the minimum flux needed to get a n -standard-deviation detection from a point-like gamma-ray source, estimated for a data taking of duration T ($n = 3$, $T = 1$ year for the project ASTROGAM, Fig. 1 and [5]). Figure 3 shows the variation of s with E for the *Fermi* LAT ($n = 5$, $T = 10$ year) [3]. Besides an increase of the effective area, A_{eff} , and/or of the mission duration, T , both of which depend heavily on the funding availability, the only way to improve on the sensitivity (decrease the value of s) is to improve on the angular resolution, σ_θ , something that has been the topic of my talk.

“We are not facing a sensitivity wall, we are facing an angular resolution wall” (I. Grenier, 2016).

Upon the conversion of an incident γ -ray “in the field” of a charged target, supposed to be at rest, a pair of e^+ and e^- leptons is created, with momenta \vec{p}_+ and \vec{p}_- , and some momentum, \vec{q} is transferred to the target that then “recoils”:

$$\vec{k} = \vec{p}_+ + \vec{p}_- + \vec{q}. \quad (1)$$

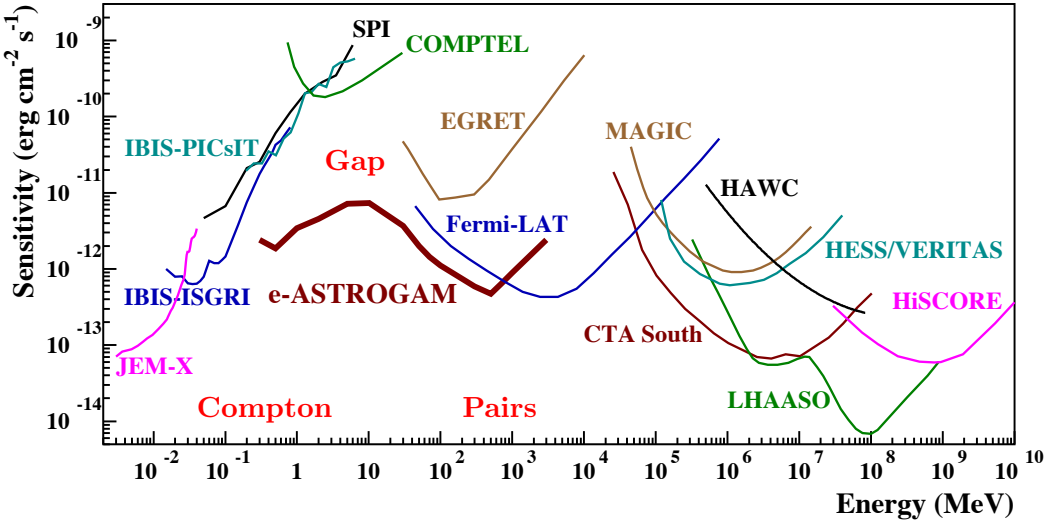


Figure 1: Expected differential continuum sensitivity of the ASTROGAM project (brown curve), compared to that of past and present X-ray and γ -ray telescopes. The Compton and Pair parts of the γ -ray realm are indicated in red, so is the **sensitivity gap** between them. Adapted from [5].

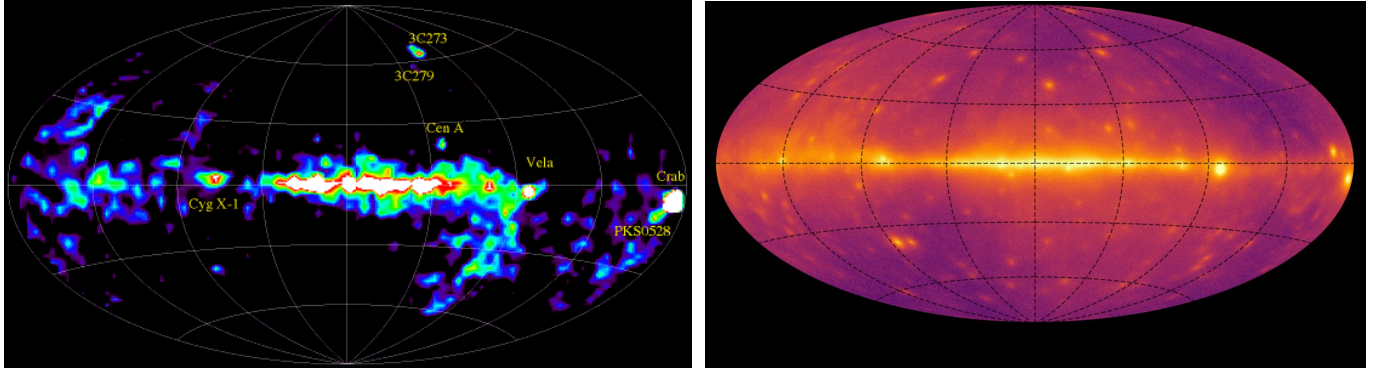


Figure 2: Maps of the γ -ray sky from the COMPTEL (left, Compton regime, 1 – 30 MeV, 9 years, [7]) and from the LAT (right, pair creation regime, 20 – 200 MeV, 13 years, [8]) telescopes.

The astronomer reconstructs the photon momentum \vec{k} from the measurement of the momenta of the particles in the final state.

- When the target is the nucleus of an atom of the detector (“nuclear conversion”), the recoil track length is too short that \vec{q} can be measured, even with a low-density (gas) tracker.
- When the target is an electron (“triplet conversion”), the track can be longer, but the cross section is lower and in practice the fraction of the events that has a recoil momentum large enough to enable a measurement is tiny (see, eg., Fig. 6 of [6]).

So ([9] and references therein), the single photon angular resolution can be broken down into the following contributions:

- (1) the fact that \vec{q} cannot be measured, a missing piece in the calculation of \vec{k} ;
- (2) the momentum resolution for each track of the pair;
- (3) the single-track angular resolution.

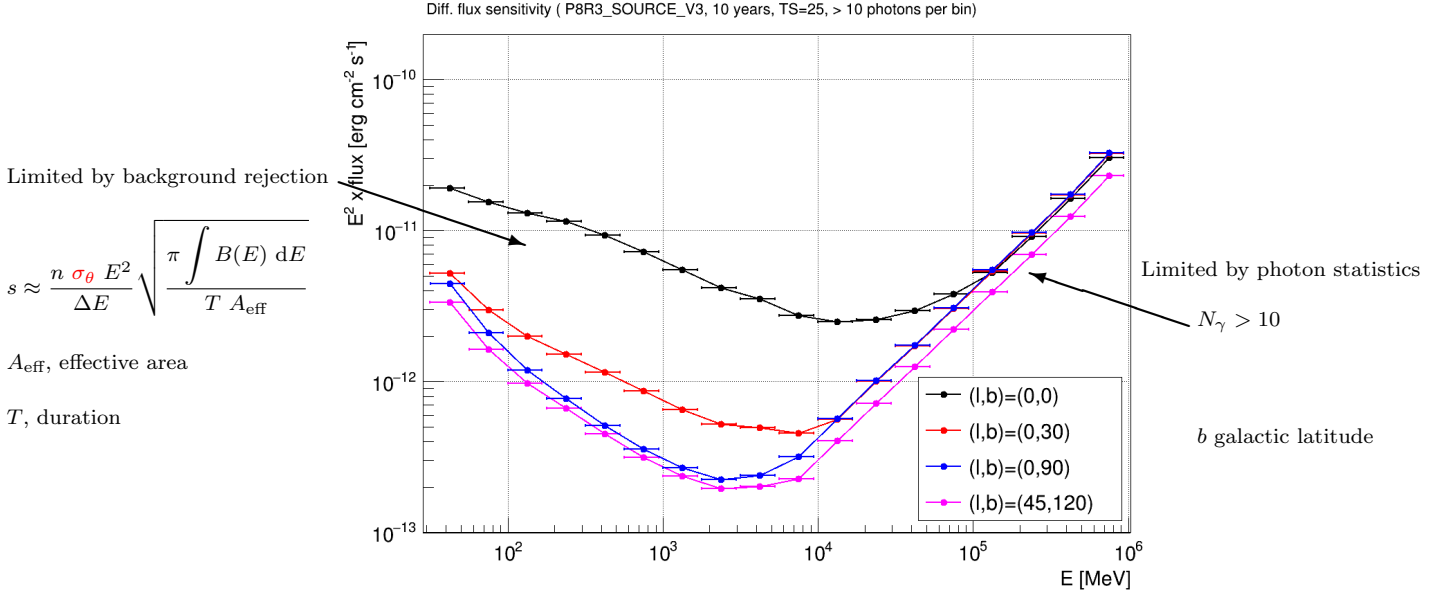


Figure 3: Differential sensitivity of the Fermi LAT [3].

2 Recoil

The direction of the recoil is found to be, asymptotically at high energy, transverse to the direction of the incident photon (see center plot in Fig. 4), so the induced angular shift of the reconstructed photon due to the missing recoil is of about¹ q/k . The distribution of the magnitude of the recoil momentum extends, in principle, asymptotically, from $q_{\min} = 2m^2/k$ up to² $q_{\max} = 2k$. In practice, though,

- the fraction of the cross section that extends above $1 \text{ MeV}/c$ is extremely small (nuclear conversion, see left plot of Fig. 4; triplet conversion, Fig. 6 of [6]);
- at high energies ($E > \text{few} \times 100 \text{ MeV}$), the lowest part of the q spectrum is suppressed by the screening of the electric field of the target by the electron “cloud” (dotted curves on the left plot of Fig. 4).

As the angular kick induced by the missing recoil in the reconstruction of the photon direction shows a strongly non-Gaussian distribution, the contribution to the angular resolution is referred to as the angle value that “contains” a fraction x of the events, with $x = 68, 95$ and 99.7% (Fig. 5 and [9, 10]). The 68% containment value can be parametrized by $\theta_{68} = 1.5 \text{ rad} (E/\text{MeV})^{-5/4}$ (the thin black line on Fig. 5) [9, 10], and amounts to 0.27° at 100 MeV .

A number of misconceptions have been published in the past on this kinematical limit of the angular resolution of pair telescopes. Recently, for example, [11] states (eq. (30), up to a trigonometric function) a $1/E$ variation, based on the allegation that “The most probable energy transfer to the nucleus is close to the energy at rest of the electron”. Actually [11] uses the Geant4 *G4EmLivermorePolarizedPhysics* list, in which, in the *G4LivermorePolarizedGammaConversionModel* physics model, the Bethe-Heitler differential cross section [13–15] is not sampled; instead the polar angles of the two leptons are taken at random independently, so given the $1/E$ (asymptotic) scaling of the distribution of the opening angle [12] (see also Fig. 6, left), the induced violation of the energy-momentum conservation in the conversion ends up in an

¹The contribution to the angular resolution, in the $\theta_{68} \approx q_{68}/k$ approximation, is found to be compatible with the exact value above a couple of MeV (Fig. 3 (right) of [10]).

²Under the approximation of $k \ll Mc^2$, M nucleus mass, that is legitimate in the context of the “MeV” session of this conference.

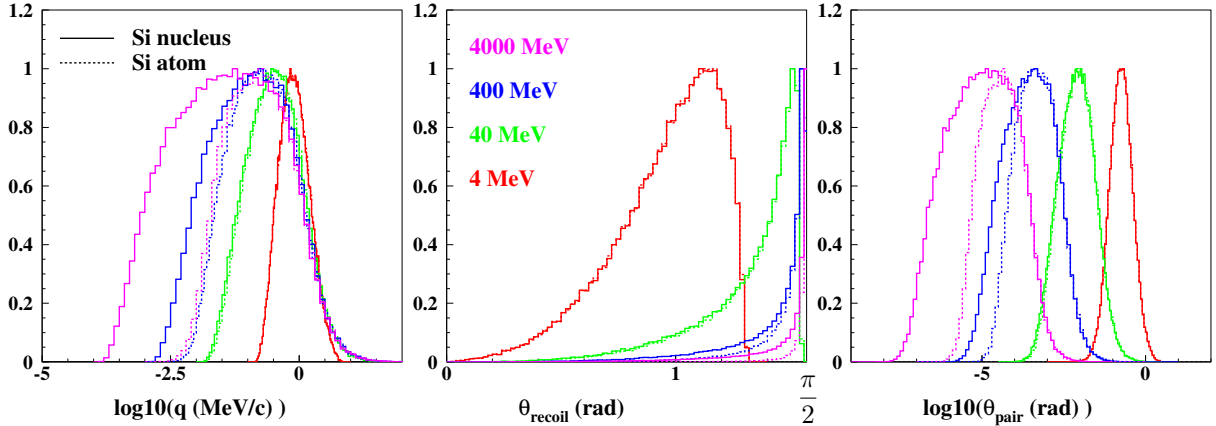


Figure 4: Target recoil in nuclear conversions of γ -rays on silicon, either on isolated nuclei (solid curves) or on full atoms (dotted curves), for several incident photon energies. Left, (log of) recoil momentum magnitude. Center, recoil polar angle. Right, (log of) the (true, not the q/k approximation) contribution of the missing recoil to the single-photon angular resolution.

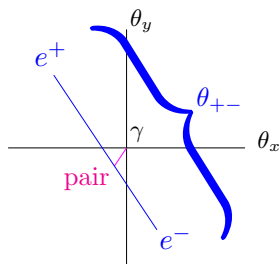
artificial, pseudo-kinematical contribution to the angular resolution that goes like $1/E$ (Figs. 10, 12 and 14 of [11]).

Similar comments can be made on alternative physics models such as *G4BetheHeitlerModel* or *G4LivermoreGammaConversionModel* for which energy (not momentum) conservation is used to correlate the polar angles of the two leptons in a coplanar, recoil-less, scheme. In that case, the induced q_{68} obviously collapses to zero (asymptotically), (magenta open circles in Figs. 6-8 of [10]).

I would like to respectfully recommend that that tools, in general, and event generators, in particular, be validated before they are used, given the specifications of the intended use³. See, eg., how the method used in *G4BetheHeitler5DModel* to sample the full (5 dimensional) Bethe-Heitler differential cross section [13–15] was validated [16, 17] before it was chosen [18] by Geant4 [19, 20] as the default physics model for the simulation of precision electromagnetic physics. For the recoil momentum distribution, which is the key point in the present discussion, the simulated distribution was validated with respect to the high-energy asymptotic expression from Jost *et al.* [21]⁴, see Fig. 4 of [9] and Fig. 2 left of [18].

3 Single-Track Momentum Resolution

Let's have a look at the final state in the plane perpendicular to the direction of the incident photon



The thin magenta segment shows the transverse kick given to the pair, back-to-back to the recoil. Unless

³As analytical expressions of the distributions of the single track polar angle and of the fraction of the energy carried away by (e.g.) the positron are available [13], the physics models that I have commented on actually provide excellent simulations of the properties of electromagnetic showers.

⁴With Borsellino's correction [22] applied.

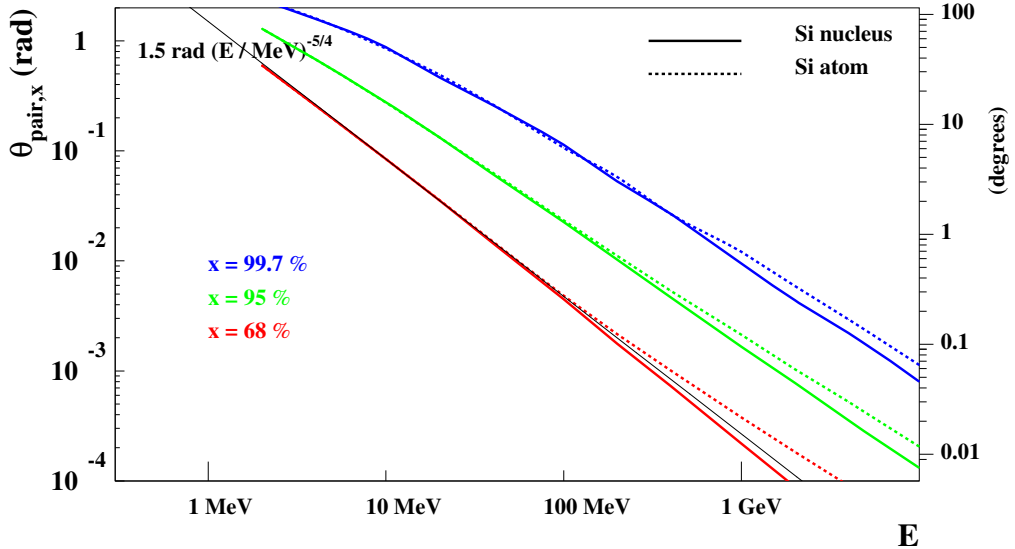


Figure 5: Variation of the contribution of the missing recoil momentum to the single-photon angular resolution for γ -ray conversions to pairs on silicon (solid line, isolated nucleus; dotted line, full atom). Values at $x = 68, 95$ and 99.7% “containment” are shown. The thin black line is a good representation of the variation for $x = 68\%$ [9, 10].

the magnitude of the momenta of the two tracks are measured, the direction of the reconstructed photon can lie anywhere on the thin blue segment that extends from the e^+ to the e^- , and the extension of which is equal to the opening angle, θ_{+-} . The distribution of θ_{+-} scales like $1/E$ asymptotically ([12] and Fig. 6 left), as we have already seen, and unfortunately it’s magnitude is huge, 5 rad(MeV/E) at 68% containment (Fig. 6 right).

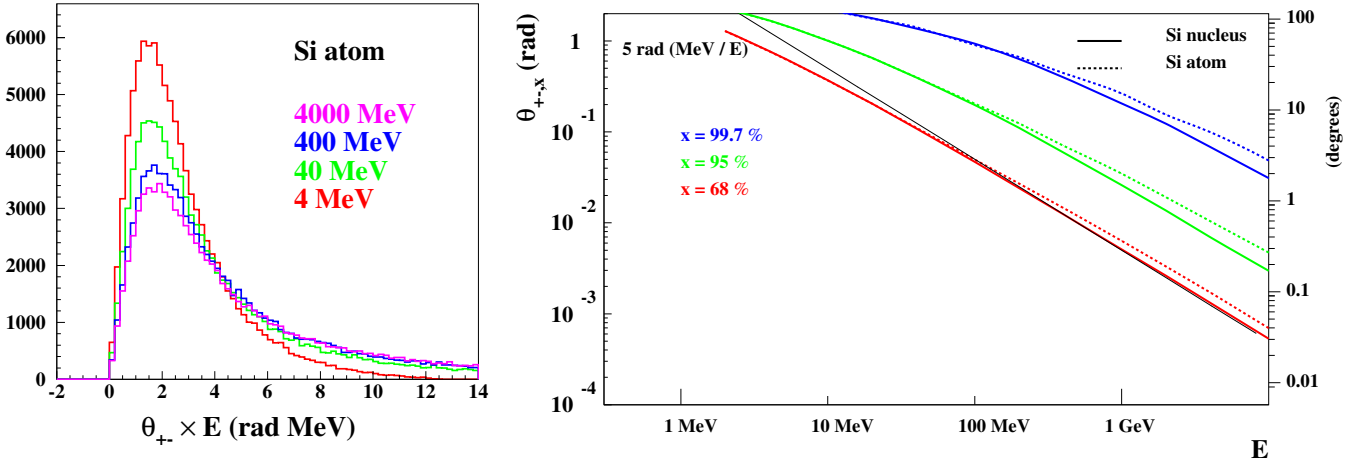


Figure 6: Pair opening angle, θ_{+-} , in γ -ray conversions on silicon. Left, distribution of $\theta_{+-} \times E$, for several values of E . Right, θ_{+-} “containment” value as a function of E . The thin black line is a good representation of the variation for $x = 68\%$.

3.1 Equipartition, bisectrix

The easiest way to deal with the issue is to assume equipartition and therefore to assign the bisectrix of the directions of the two leptons as the direction of the reconstructed photon. Figure 7 shows the contributions

to the angular resolution (containment values) of

- the angle between the true and the reconstructed pair momentum assuming equipartition ($\theta_{(\text{pair}, \text{bisectrix})}$, thin curve),
- the already mentioned contribution of the missing recoil momentum, ie., the angle between the true pair momentum and the incident photon direction ($\theta_{(\text{photon}, \text{pair})}$, medium thickness) and their combination, into
- the full angular resolution, ie., the angle between the reconstructed pair momentum assuming equipartition and the incident photon direction ($\theta_{(\text{photon}, \text{bisectrix})}$, thick curve).

We see that $\theta_{(\text{pair}, \text{bisectrix})}$ dominates over $\theta_{(\text{photon}, \text{pair})}$, for $E > 10 \text{ MeV}$.

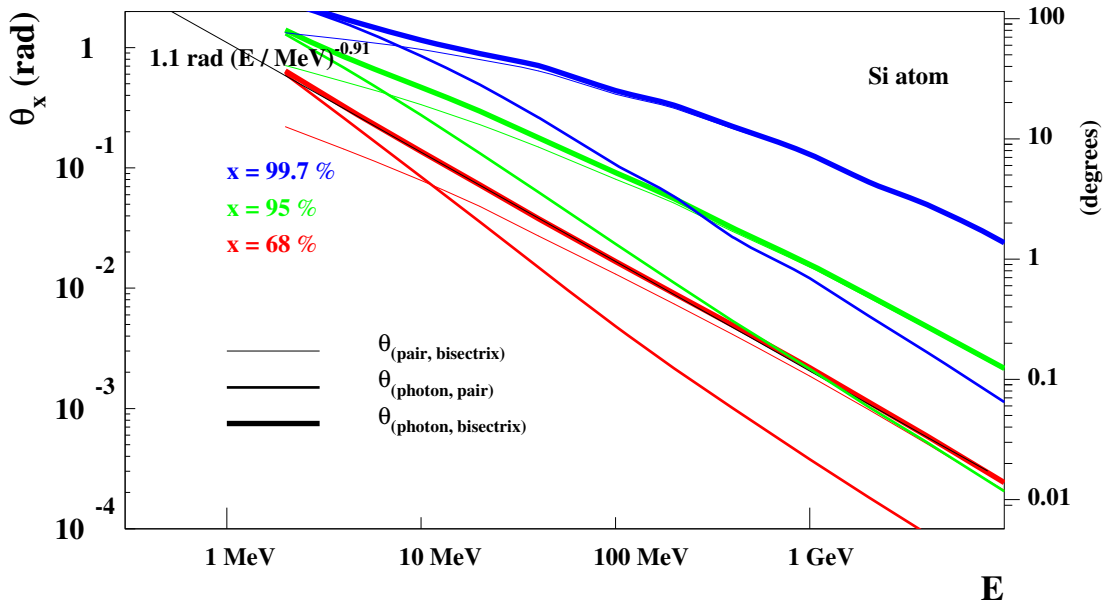


Figure 7: Contributions to the single-photon angular resolution assuming equipartition ($p_+ = p_-$).

- The angle between the true and the reconstructed pair momentum ($\theta_{(\text{pair}, \text{bisectrix})}$, thin curve),
- the angle between the true pair momentum and the incident photon direction ($\theta_{(\text{photon}, \text{pair})}$, medium thickness),
- the angle between the reconstructed momentum and the incident photon direction ($\theta_{(\text{photon}, \text{bisectrix})}$, thick curve).

Values at $x = 68, 95$ and 99.7% “containment” are shown. The thin black line is a good representation of the variation for $x = 68\%$.

3.2 Measurement of the magnitude of the track momentum

Several methods can be used, though, external to the tracker/converter, to measure either the momentum or the energy of each track⁵, but at the cost of a heavy impact of the mass budget of the mission:

Calorimeter	Calorimeter	Calorimeter	Magnetic spectrometer
Fermi LAT [3]	ASTROGAM [24]	AMEGO [23]	AMS-02 [25]
CsI(Tl) ($8.6 X_0$)	CsI(Tl) ($4.3 X_0$)	CsI(Tl)	Magnet + Si tracker
$\sigma_E/E = 20\% @ 100 \text{ MeV}$	$\sigma_E/E = 20 - 30\% @ > 30 \text{ MeV}$	17% at 100 MeV	$\sigma_p/p = 14\% @ 200 \text{ MeV}$
(68%)		(68% containment half width)	

⁵I assume that the photon energy resolutions quoted in the following table apply also to each track independently.

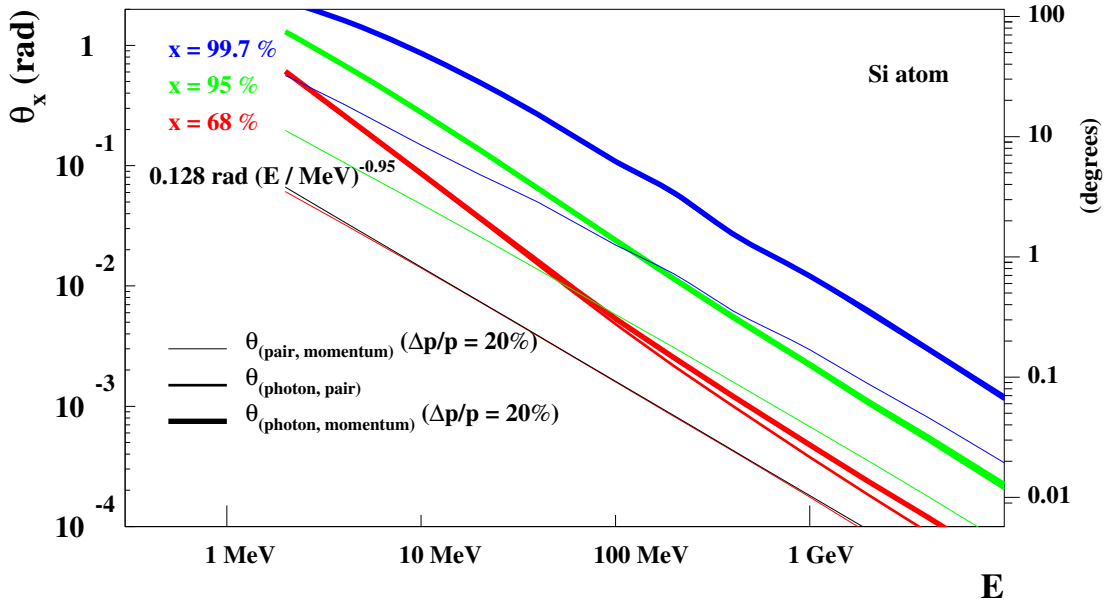


Figure 8: Contribution to the single-photon angular resolution assuming a $\sigma_p/p = 20\%$ single-track relative momentum resolution. The thin black line is a good representation of the variation for $x = 68\%$.

The track momenta can also be measured from the information collected by the tracker/converter itself; as the RMS angle deflection undergone from multiple scattering by a charged particle in its way through a detector is inversely proportional to its momentum, the momentum can be inferred from an analysis of the deflections [26, 27]. This method was used in emulsion-based γ telescopes with a typical relative momentum resolution of 10 to 20 % [28].

Assuming an RMS relative momentum resolution of σ_p/p of 20 %, the contribution to the photon angular resolution is obviously found to be better than when assuming equipartition. Figure 8 shows

- the contribution of a 20 % relative momentum resolution ($\theta_{(\text{pair,momentum})}$), thin curve), and
- the already mentioned contribution of the missing recoil momentum ($\theta_{(\text{photon,pair})}$, medium thickness) compared and combined, into
- the full angular resolution, assuming a 20 % relative momentum resolution ($\theta_{(\text{photon,momentum})}$, thick curve).

The 68 % containment value, that can be parametrized by $0.64 \text{ rad} (\sigma_p/p) (E/\text{MeV})^{-0.95}$, is found to be negligible when compared to the recoil contribution, on the whole photon energy range.

3.3 Interim wrap-up, (1)+(2)

At this point, let's attempt an interim wrap-up comparing the predictions for the two contributions examined up to now, (1)+(2), to the angular resolutions of the present telescopes and future projects (Fig. 9).

- The angular resolutions for all telescopes are found to be larger than the predictions.
- For the telescopes for which the photon direction was reconstructed using the measured value of the track momenta (GRAINE, eq. (3.1) of [29]; ASTROGAM, eq. (1) of [11]; AMEGO-X, H. Fleischhacker, private communication), it is interesting to note that, instead, their resolutions would rather be compatible with the prediction for equipartition.

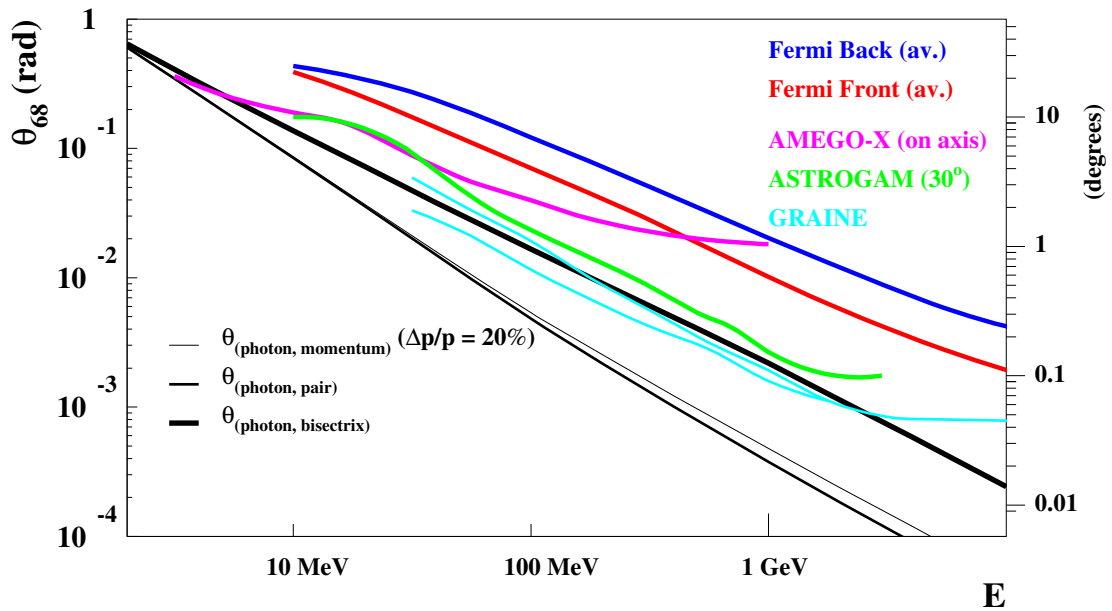


Figure 9: Telescope single-photon angular resolution as a function of E for the Fermi LAT [3], GRAINE, [30], AMEGO-X, [23] and ASTROGAM, [24], compared to the full (including the recoil) resolution assuming a $\sigma_p/p = 20\%$ single-track relative momentum resolution, ($\theta_{\text{photon,momentum}}$, thick curve), the contribution of the missing recoil momentum ($\theta_{\text{photon,pair}}$, medium thickness) and the full resolution assuming equipartition ($\theta_{\text{photon,bisectrix}}$, thick curve).

3.4 Optimal track momentum measurement

An optimal measurement of the track momentum can be obtained from a bayesian analysis of the innovations of a Kalman-filter-based track fit applied to the track [31]. Let's consider a converter/tracker consisting of a series of N layers, with a spacing ℓ , and scatterer thickness Δ with radiation length X_0 , with a track position precision σ for each layer; (for an homogeneous detector, $\Delta = \ell$).

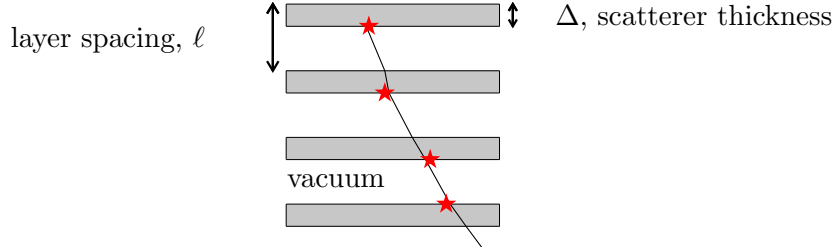


Figure 10: Schema of a converter/tracker.

The value of the track momentum is obtained [31] from the value of s , the average multiple-scattering angle variance per unit track length,

$$s \equiv \left(\frac{p_0}{p} \right)^2 \frac{\Delta}{\ell X_0}, \quad (2)$$

that maximizes the Kalman filter innovation probability density function (Fig. 11, left). $p_0 = 13.6 \text{ MeV}/c$ is the multiple scattering constant [32].

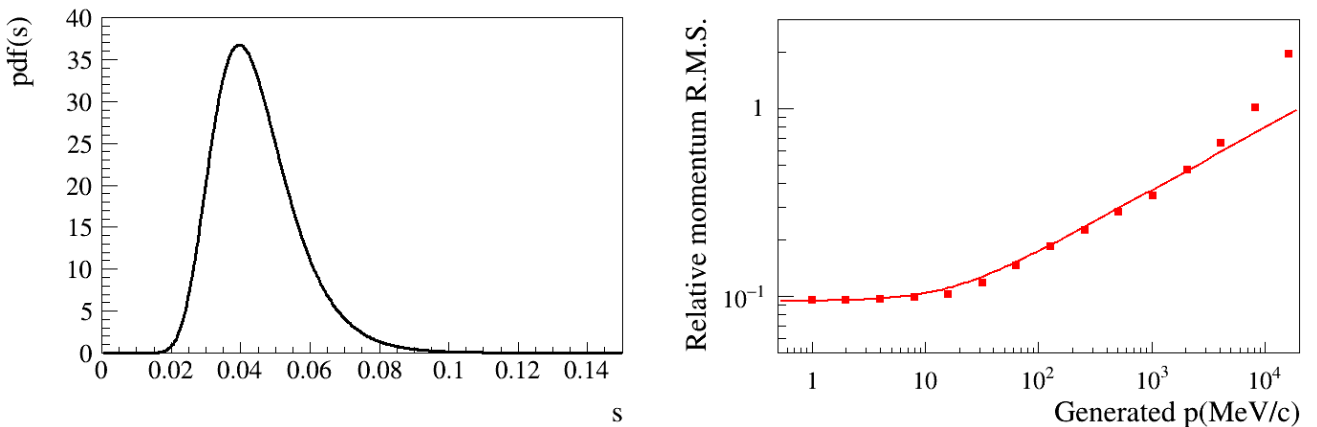


Figure 11: Internal (to the tracker/converter) optimal track-momentum measurement from the analysis of the multiple deflections induced by multiple scattering, for a DSSD tracker/converter (ASTROGAM) [31]. Left, Kalman filter innovation probability density function as a function of s , the average multiple-scattering angle variance per unit track length, for a $50 \text{ MeV}/c$ track. Right, relative momentum resolution as a function of (true) track momentum; the curve shows the parametrization of eq. (3).

A good representation of the relative precision of the measurement (curve in Fig. 11, right) is given by (eq. (58) of [31])

$$\frac{\sigma_p}{p} \approx \frac{1}{\sqrt{2N}} \sqrt[4]{1 + 256 \left(\frac{p}{p_0} \right)^{4/3} \left(\frac{\sigma^2 X_0}{N \Delta \ell^2} \right)^{2/3}}, \quad (3)$$

A quantity of interest is, $p_{1/2}$, the momentum above which σ_p/p is larger than $1/2$, which means that

the measurement becomes meaningless [31]:

$$p_{1/2} = p_0 \frac{N^2}{32^{3/2}} \left(\frac{\ell}{\sigma} \right) \left(\frac{\Delta}{X_0} \right)^{1/2}. \quad (4)$$

For ASTROGAM, the method is usable on our whole energy range, with $p_{1/2} = 2.5 \text{ GeV}/c$ (Fig. 11).

The method should be usable for the GRAINE tracker/converter too, on most of the MeV energy range (Fig. 12).

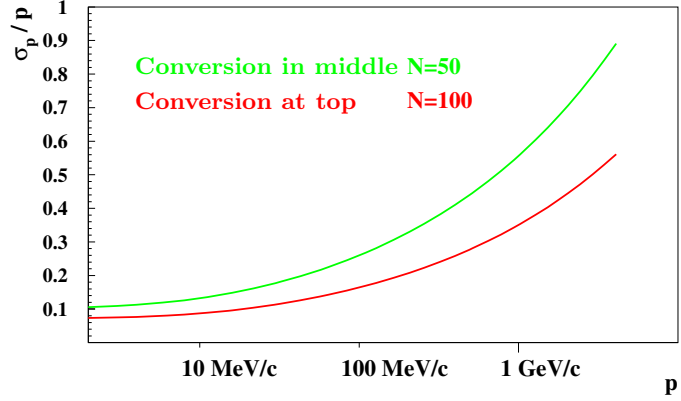


Figure 12: *Internal optimal track momentum measurement from the analysis of the multiple deflections induced by multiple scattering, applied to the emulsion-based tracker/converter of the GRAINE project, as computed with eq. (3).*

4 Single-Track Angular Resolution

I now examine the last (but not least, alas) contribution to the single-photon angular resolution, that is, the single-track angular resolution. Tracking, the determination of a parametrization of the trajectory of a track in a tracker, and in particular of its direction at the vertex (the beginning of the track) is a challenging issue, as the space resolution of each tracker layer and the multiple scattering (MS) contribute together, and because MS deflections induce correlations in the measured positions in layers downstream to the position where they took place. An optimal way out is the use of a Kalman filter applied to the track measurements [33], a recursive process that combines

- an optimal estimate of the “state” of the track at layer i (and its variance matrix),
- and the measurement at layer $i + 1$ (and its variance matrix),
- into an optimal estimate of the “state” at layer $i + 1$ (and its variance matrix).

In a scheme of successive (scatter), (measurement), (drift in empty space) steps, we consider first a track originating from a vertex located at the very bottom of a layer (Fig. 10), that is, (measurement) then (drift), and then only (scattering). An analytical expression of the precision of such a tracking has been obtained in [31] (see the validation plot in Fig. 8 of [31] but the published expression in [31] has a misprint). We have (eq. (1) of [34])

$$\sigma_\theta = \frac{\sigma}{\ell} \sqrt{\frac{2x^3 \left(\sqrt{4j - x^2} + \sqrt{-4j - x^2} \right)}{\left(\sqrt{4j - x^2} + jx \right) \left(\sqrt{-4j - x^2} - jx \right)}}, \quad (5)$$

where x is the distance between layers, ℓ , normalized to the detector scattering length λ (defined in eq. (17) of [31], see also [35]), $x \equiv \ell/\lambda = \sqrt{(\ell/\sigma)(p_0/p)\sqrt{\Delta/X_0}}$, σ is the precision of the measurement of the track position in a layer, and j is the imaginary unit. Contrary to appearances, σ_θ turns out to be a real quantity, which is good. The variation of σ_θ with p (Fig. 13) shows two regimes⁶:

- at low momentum (large x), the coarsely-segmented detector approximation can be used, with the obvious

$$\sigma_\theta \approx \sqrt{2}\sigma/\ell, \quad (6)$$

that is, an optimal measurement can be obtained simply from the position measurements in the two first wafers, no Kalman filter is needed.

- at high momentum (small x), the power of the Kalman filter kicks in, and the homogeneous detector approximation [6] can be used,

$$\sigma_\theta \approx (p/p_1)^{-3/4}, \quad (7)$$

where p_1 is a momentum that characterizes the tracking-with-multiple-scattering properties of the detector (eq. (17) of [6], eq. (38) of [31]).

$$p_1 = p_0 \left(\frac{2\sigma}{\ell} \right)^{1/3} \left(\frac{\Delta}{X_0} \right)^{1/2}. \quad (8)$$

The frontier between the realms of the segmented detector and the homogeneous detector can be defined by the crossing of the two asymptotes, p_f (vertical [line](#) in Fig. 13)

$$p_f = p_0 \sqrt{\frac{\Delta}{X_0}} \frac{\ell}{\sigma 2^{1/3}}. \quad (9)$$

⁶At much higher momenta, that is, outside the scope of this paper, multiple scattering becomes negligible, and tracking boils down to the fit of a straight line ($\vec{B} = 0$) or of an helix ($\vec{B} \neq 0$), with a single-track angular resolution at vertex of $\sigma_{\theta t} \approx (2\sigma/L)\sqrt{3/(N+5)}$ and $\sigma_{\theta t} \approx (8\sigma/L)\sqrt{3/(N+5)}$, respectively [36].

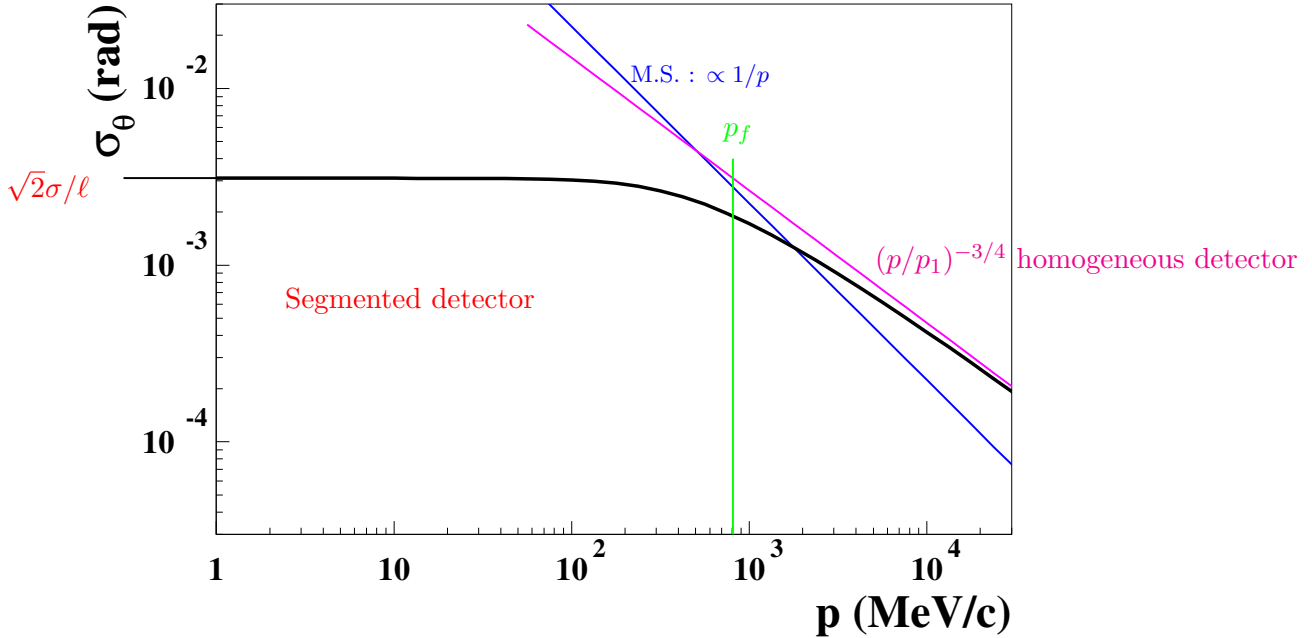


Figure 13: Single track angular resolution for a vertex located at the very bottom of a layer, for the front part of the Fermi LAT, as a function of track momentum. The black curve is from eq. (5), see also [34]. The **low momentum (segmented detector)** (eq. (6)) and the **high-momentum (homogeneous detector)** (eqs. (7), (8)) asymptotes are shown, together with the **frontier** (vertical line, eq. (9)) between them. In addition, the RMS deflection from multiple scattering through a full layer (**M.S.**) is drawn.

The numerical values of p_1 , $p_{1/2}$ and of p_f for the detector test cases considered in this work can be found in Table 1.

When conversion takes place within the fat of a layer, instead of the very bottom of it, the contribution of multiple scattering in the conversion layer must be taken into account in addition (blue line in Fig. 13, for a full layer).

4.1 From single-track angular resolution to single-photon angular resolution

The energy dependence of the single-photon angular resolution induced by a momentum dependent single-track angular resolution has been studied in Fig. 1 of [9]. Here I assume that the momentum dependence for the tracks translates directly to the same energy dependence for the photons.

Table 1: Parameters of the text case telescopes considered in this work.

<i>Fermi</i> LAT [37]		ASTROGAM [24]	AMEGO [23]	GRAINE [28, 29]				
N	$2 \times$ SSSD + W foils	Front	Back	DSSD	pixels	emulsions		
ℓ	12	4	56		60	Automatic	35 (b)	number of layers
Δ	3	3	1		1		0.0004 (b)	spacing between layers
X_0	95	720	500		500		4 (b)	scatterer thickness
p	W	W	Si		Si	film	film	scatterer nature
σ	0.35	0.35	9.37		9.37	2.84	2.84	scatterer radiation length
p_1	228	228	240		1000			pitch
$p_{1/2}$	66 (a)	66 (a)	70 (a)		290 (a)		0.060	single layer space resolution
p_f	0.37	1.0	0.24		0.38		0.045	detector “scattering” momentum eq. (8)
	812.	248.	2460.		684.		25.7	momentum for which $\sigma_p/p = 1/2$ eq. (4)
	810.	2230.	113.		27.		3.0	frontier between the low and high energy asymptotes of the track angular resolution, eq. (9)

(a) $\sigma = p/\sqrt{12}$

(b) Poisson distributed, from the average count density of 50 counts / 100 microns.

4.2 Telescope Test Cases

At this point, it’s time to gather details on the tracker/converter of the telescope test cases considered in this work (Table 1).

- The tracker of the LAT consists of pairs of single-sided silicon strip detectors, located just below a high- Z material (tungsten) foil, with thinner foils in an upper “front” set and thicker ones in a “back” set [37].
- The tracker of the ASTROGAM project consists of 56 planes of double-sided silicon strip detectors [24].
- The “historical” AMEGO project has been similar to ASTROGAM, but in its most recent version, AMEGO-X [23], strips have been changed to pixels, so as to decrease the capacitance of individual detector elements, so that the low electronic noise enables an improved sensitivity for very-low-energy Compton events. This at the cost of an enlarged pitch of 1mm.
- The tracker/converter of the GRAINE project consists of 100 films, with a total thickness of 3 cm, each film consisting of two emulsions on both sides of a transparent base [28, 29]. High-density emulsions are used with an average count density of 50 counts / 100 microns. Events can be reconstructed in two ways:
 - either films are scanned by an automatic machine, in which case the track direction is computed from the position measured in the upper and of the lower emulsion layers of the first film⁷. The relative positioning precision upon scanning is of about 0.42 μm . The angular resolution is shown as the cyan [upper curve](#) in Fig. 9.
 - or, the film is scanned by an operator with a microscope and the position of each grain is determined with a precision of 0.060 μm ; The angular resolution is shown as the cyan [lower curve](#) in Fig. 9. The small value of $p_1 = 45 \text{ keV}/c$ makes GRAINE well suited for high-performance γ -ray polarimetry (see Fig. 20 of [6]) as demonstrated by the characterization of a prototype on a polarized γ -ray beam [38].

⁷Multi-film measurements improve the angular resolution at GeV energies, i.e., outside the scope of this work, see Fig. 3 of [30].

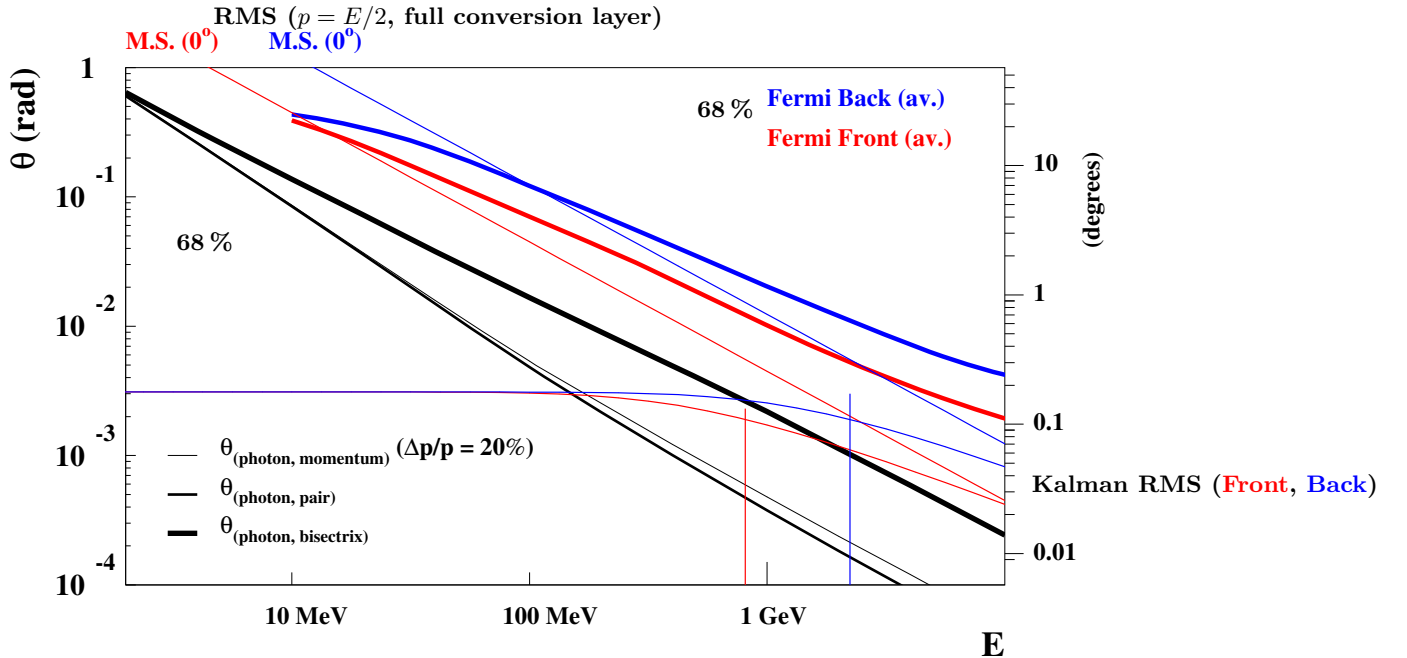


Figure 14: The angular resolution of the *Fermi LAT* (**front**, **back**), averaged on the telescope solid angle acceptance [3], compared to the contributions studied in this work. The “bisectrix” curve is shown even though the reconstruction of the *LAT* data does not use that method. The parametrization of the angular resolution of a Kalman filter on track that would traverse the full (either **front** or **back**), computed from eq. (5), is also drawn, together with the values of p_f (vertical lines).

5 Discussion

Fermi LAT

The angular resolutions for the front and for the back part of the *Fermi LAT* (Fig. 14) are vaguely compatible with the multiple scattering inside the conversion layer (drawn for an incident photon at 0° and for a full layer), all other contributions considered in this work being completely negligible. In particular the use of a Kalman filter would be useless on our energy range.

It should be noted, though, that the slope (in log-log coordinate) of the data, close to -0.8 , is quite different from that of multiple scattering (that is, -1). This might be due to the fact that the critical energy, E_c of the *LAT*, that is, the energy for which the limit pair opening angle that can be measured from the two first layers, $\theta_c = p/\ell$ is equal to the most probable pair opening angle [39], is equal to 211 MeV, so the transition between

- a low energy regime for which most events have, in the second layer, the two tracks hit separate strips, and
- a high-energy regime in which most events have the two tracks hit the same strip,

falls right into our energy range. Further more; the present event reconstruction, PASS 8 [40], is strongly based on the reconstruction of one main track, in a scheme somewhat different of what considered here.

“Pure-silicon”

The projects ASTROGAM and AMEGO-X, (Fig. 15), are also dominated by multiple scattering in the conversion wafer with a bizarre shape in the tens of MeV maybe related to the values of the critical energies (67 MeV for ASTROGAM; 16 MeV for AMEGO-X); (The bisectrix curve is drawn for reference but neither project is using the method, as far as I know.)

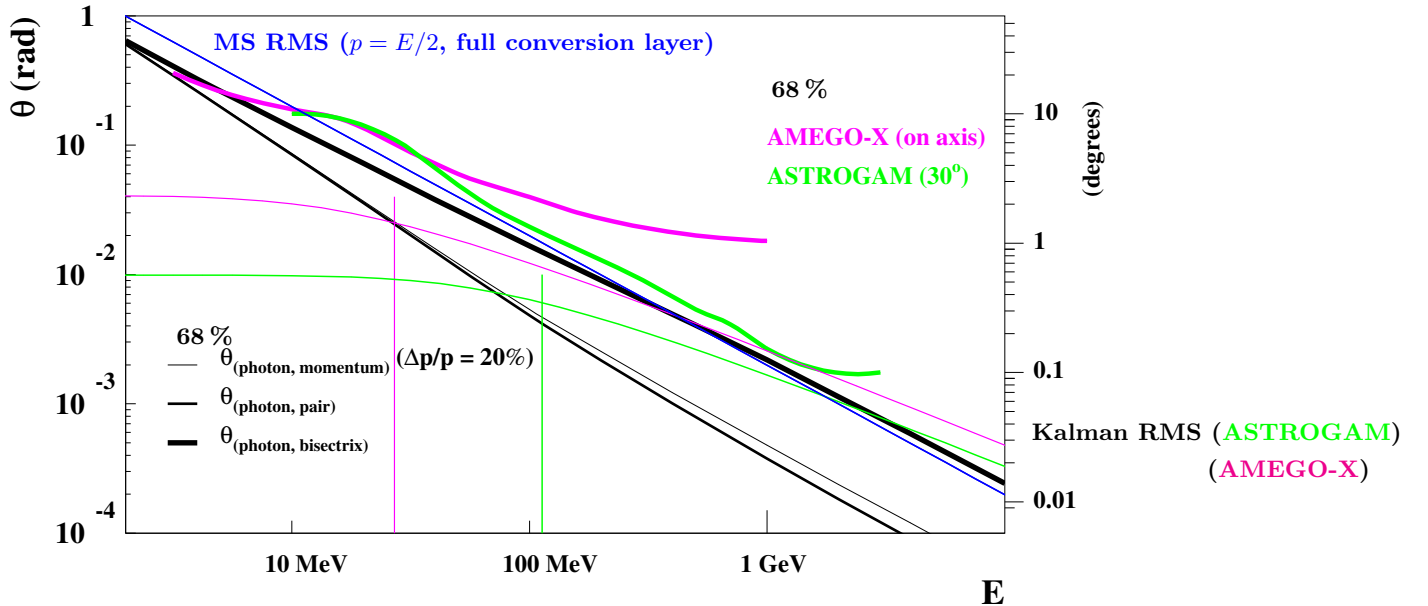


Figure 15: The angular resolution of the “pure silicon” projects, **AMEGO-X** and **ASTROGAM** compared to the contributions studied in this work. The “bisectrix” curve is shown even though the reconstruction of the LAT data does not use that method. The parametrization of the angular resolution of a Kalman filter on track that would traverse the full detector, computed from eq. (5), is also drawn, together with the values of p_f (vertical lines).

As the Kalman filter is equivalent to a two-point measurement at low energies ($p_f = 113 \text{ MeV}/c$ for ASTROGAM, $p_f = 27 \text{ MeV}/c$ for AMEGO-X), the ability to assign the momenta (excellently) measured in the rest of the event to the correct strip or pixel cluster in the second layer is also key to a correct momentum weighting, similarly to the discussion of the limits of track matching for the LAT at the end of section 6 of [39].

GRAINE

For GRAINE, the performance of the automatic method is well understood from multiple scattering in the first film (cyan curve in Fig. 16).

With the grain-by-grain method, the tracker is so precise that the performance should reach the kinematical limit up to a couple of hundreds of MeV, but their results are a bit larger than that. The use of a Kalman filter may bring some improvement.

6 Conclusion

I studied several contributions to the single-photon angular resolution of pair telescopes in the MeV energy range, by numerical methods.

The main strength of the study lies in the use of a validated sampling of the exact, that is 5D, Bethe-Heitler differential cross section, which is key to the understanding of the distribution of the (direction and magnitude) of the target recoil momentum, and of the pair opening angle, the properties of which impact heavily the photon angular resolution.

The contribution of the resolution of the magnitude of the momenta of the tracks, σ_p/p is found to be proportional to σ_p/p , and for a mild assumption of $\sigma_p/p = 0.2$, is found to be smaller than the kinematical limit of the unmeasured target recoil.

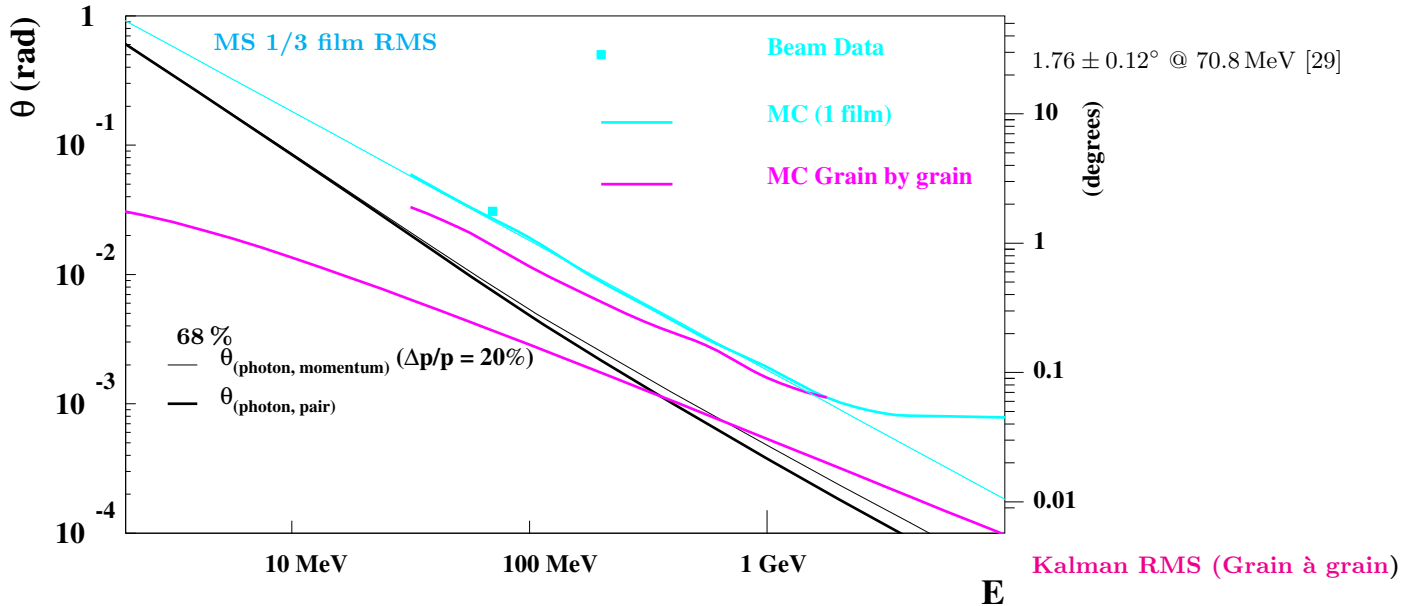


Figure 16: The angular resolution of the GRAINE project, either with the [automatic scanning](#) or with the [grain-by-grain](#) method, compared to the contributions studied in this work. The “bisection” curve is shown even though the reconstruction of the LAT data does not use that method. The parametrization of the angular resolution of a Kalman filter on track that would traverse the full detector, computed from eq. (5), is also drawn.

Multiple scattering was found to be the major issue, as was expected. The use of a Kalman filter, in the hope of obtaining a better determination of the photon direction than with a simple two-point measurement, is found to be useless at low energies for silicon trackers (below $\approx p_f$). A Bayesian analysis of the filtering innovations of a Kalman filter, though, provide an optimal measurement of track momenta, from the multiple deflections of the tracks in the tracker due to multiple scattering, that is sensitive on most of the energy range (below $p_{1/2}$).

The emulsion-based GRAINE project stands out, especially when the data are analyzed with the grain-by-grain method. The tiny value of the detector scattering momentum, $p_1 = 45 \text{ keV}/c$, paves the way to a high-quality γ -ray polarimetry. If a Kalman filter could be applied to the grain-by-grain data, the angular resolution could most likely reach the kinematical limit.

A number of simplifying assumptions limit the scope of this study, and a caveat is in order; radiation (bremsstrahlung) and energy loss of charged particles in the tracker (dE/dx) are not considered, something that has an important impact at the lowest energies (the assumption of a track being measured in the full N planes should be reconsidered); also the effect of multiple scattering increases while the particle is loosing energy. Most often, conversions at the top of the tracker is implied, with a contribution of the maximum number of layers, the same for all events. And as mentioned in the text already, no pattern recognition algorithm is used, so the transverse discretization of the reading of the signal in strip- or pixel-segmented trackers, with the associated issue of a pair of tracks possibly contributing to the same single cluster in the second layer, is out of the scope of the present work based on the presence of two well-identified tracks. Also various definitions of the resolution, RMS or 68 % containment value, have been used equivalently.

Never the less, I hope that the work will be of some use, in particular as a guide for designers for future γ -ray telescopes.

7 Acknowledgements

My gratitude to the organizers of the 2023 International Conference of Deep Space Sciences for their kind invitation and to Simone Maldera (*Fermi* LAT), Regina Caputo and Henrike Fleischhack (AMEGO-X), and Satoru Takahashi (GRAINE) for their help during the preparation of my talk.

Contents

1	Introduction	1
2	Recoil	3
3	Single-Track Momentum Resolution	4
3.1	Equipartition, bisectrix	5
3.2	Measurement of the magnitude of the track momentum	6
3.3	Interim wrap-up, (1)+(2)	7
3.4	Optimal track momentum measurement	9
4	Single-Track Angular Resolution	11
4.1	From single-track angular resolution to single-photon angular resolution	12
4.2	Telescope Test Cases	13
5	Discussion	14
6	Conclusion	15
7	Acknowledgements	17

A_{eff}	effective area
$B(E)$	background differential flux
ΔE	incident photon energy bin
Δ	scatterer thickness
E	incident photon energy
E_c	critical photon energy
k	incident photon momentum
ℓ	distance between layers (i.e. track longitudinal sampling)
λ	detector scattering length
m	electron mass
M	nucleus mass
n	number of standard deviations (in definition of the sensitivity)
N	number of layers of the tracker/converter
p	momentum
q	“recoil” momentum transferred to the target
s	sensitivity
s	the average multiple-scattering angle variance per unit track length
σ	R.M.S.
T	duration
θ	polar angle (respective to the direction of the incident photon)
θ_{+-}	pair opening angle
x	containment fraction
x	distance between wafers normalized to the detector scattering length, $x \equiv \ell/\lambda$
X_0	radiation length

References

- [1] R. Rando, “The *Fermi* Large Area Telescope,” invited chapter for Handbook of X-ray and Gamma-ray Astrophysics (Eds. C. Bambi and A. Santangelo, Springer Singapore, [arXiv:2208.13635 [astro-ph.IM]]).
- [2] S. Abdollahi *et al.* [Fermi-LAT], “Incremental *Fermi* Large Area Telescope Fourth Source Catalog,” *Astrophys. J. Supp.* **260** (2022) 53
- [3] “*Fermi* LAT Performance”, Pass 8 Release 3 Version 3, (html)
- [4] C. Winkler *et al.*, “The INTEGRAL mission”, *A&A* 411 (1) L1-L6 (2003)
- [5] A. De Angelis *et al.* [e-ASTROGAM], “Science with e-ASTROGAM: A space mission for MeV–GeV gamma-ray astrophysics,” *JHEAp* **19** (2018), 1-106
- [6] D. Bernard, “Polarimetry of cosmic gamma-ray sources above e^+e^- pair creation threshold”, *Nucl. Instrum. Meth. A* **729** (2013) 765.
- [7] 1 to 30 MeV All-Sky Map, CGRO Science Support Center.
- [8] L. Marcotulli *et al.*, [The Fermi LAT Collaboration], “Bridging the Gap - The first sensitive 20-200 MeV catalog”, Tenth International *Fermi* Symposium, Johannesburg South Africa, 9-15 Oct 2022 (html)
- [9] D. Bernard, “TPC in gamma-ray astronomy above pair-creation threshold,” *Nucl. Instrum. Meth. A* **701** (2013) 225, Erratum: [Nucl. Instrum. Meth. A **713** (2013) 76].
- [10] P. Gros and D. Bernard, “ γ -ray telescopes using conversions to electron-positron pairs: event generators, angular resolution and polarimetry,” *Astropart. Phys.* **88** (2017) 60.
- [11] A. Aboudan *et al.*, “A Multimission Method for the Reconstruction of Gamma-ray Events on Silicon Tracker Pair Telescopes,” *Astrophys. J.* **928** (2022) no.2, 141
- [12] H. Olsen, “Opening Angles of Electron-Positron Pairs”, *Phys. Rev.* **131** (1963) 406.
- [13] H. Bethe and W. Heitler, “On the Stopping of Fast Particles and on the Creation of Positive Electrons”, *Proceedings of the Royal Society of London A*, **146** (1934) 83.
- [14] T. H. Berlin and L. Madansky, “On the Detection of gamma-Ray Polarization by Pair Production”, *Phys. Rev.* **78** (1950) 623.
- [15] M. M. May, “On the Polarization of High Energy Bremsstrahlung and of High Energy Pairs”, *Phys. Rev.* **84** (1951) 265.
- [16] D. Bernard, “A 5D, polarised, Bethe-Heitler event generator for $\gamma \rightarrow e^+e^-$ conversion”, *Nucl. Instrum. Meth. A* **899** (2018) 85
- [17] I. Semeniouk and D. Bernard, “C++ implementation of Bethe-Heitler, 5D, polarized, $\gamma \rightarrow e^+e^-$ pair conversion event generator,” *Nucl. Instrum. Meth. A* **936** (2019) 290
- [18] V. Ivanchenko *et al.* [Geant4], “Progress of Geant4 electromagnetic physics developments and applications,” *EPJ Web Conf.* **214** (2019) 02046
- [19] S. Agostinelli *et al.* [GEANT4 Collaboration], “GEANT4: A Simulation toolkit,” *Nucl. Instrum. Meth. A* **506** (2003) 250.
- [20] J. Allison *et al.*, “Recent Developments in Geant4,” *Nucl. Instrum. Meth. A* **835** (2016) 186.
- [21] R. Jost *et al.*, “Distribution of Recoil Nucleus in Pair Production by Photons,” *Phys. Rev.* **80** 189 (1950) 189.
- [22] A. Borsellino, “Momentum Transfer and Angle of Divergence of Pairs Produced by Photons”, *Phys. Rev.* **89** (1953) 1023.
- [23] R. Caputo *et al.*, “All-sky Medium Energy Gamma-ray Observatory eXplorer mission concept,” *J. Astron. Telesc. Instrum. Syst.* **8** (2022) no.4, 044003

- [24] A. De Angelis *et al.* [e-ASTROGAM], “The e-ASTROGAM mission,” *Exper. Astron.* **44** (2017) no.1, 25
- [25] B. Beischer, “Measurement of High Energy Gamma Rays from 200 MeV to 1 TeV with the Alpha Magnetic Spectrometer on the International Space Station,” CERN-THESIS-2020-065 [arXiv:2007.08392 [astro-ph.HE]]. *Ph D* (2020)
- [26] G. Molière, “Theorie der Streuung schneller geladener Teilchen. III. Die Vielfachstreuung von Bahnspuren unter Berücksichtigung der statistischen Kopplung”, *Zeitschrift Naturforschung A* **10** (1955) 177.
- [27] K. Kodama *et al.* “Detection and analysis of tau neutrino interactions in DONUT emulsion target,” *Nucl. Instrum. Meth. A* **493** (2002) 45
- [28] S. Takahashi *et al.*, “GRAINE project: The first balloon-borne, emulsion gamma-ray telescope experiment,” *PTEP* **2015** (2015) 043H01.
- [29] K. Ozaki, “Development of an emulsion telescope system for gamma-ray source observations and realization of the GRAINE 2015 balloon-borne experiment in Australia”, D1006569, Ph. D. 2016, Kobe University
- [30] S. Takahashi *et al.* [GRAINE], “GRAINE project, prospects for scientific balloon-borne experiments,” *Adv. Space Res.* **62** (2018), 2945
- [31] M. Frosini and D. Bernard, “Charged particle tracking without magnetic field: optimal measurement of track momentum by a Bayesian analysis of the multiple measurements of deflections due to multiple scattering,” *Nucl. Instrum. Meth. A* **867** (2017) 182.
- [32] R. L. Workman *et al.* [Particle Data Group], “Review of Particle Physics,” *PTEP* **2022** (2022) 083C01
- [33] R. Frühwirth, “Application of Kalman filtering to track and vertex fitting,” *Nucl. Instrum. Meth. A* **262** (1987) 444.
- [34] D. Bernard, “Performance of the MeV gamma-ray telescopes and polarimeters of the future. $\gamma \rightarrow e^+e^-$ in silicon-detector active targets,” *Mem. Soc. Ast. It.* **90** (2019) 149
- [35] W. R. Innes, “Some formulas for estimating tracking errors,” *Nucl. Instrum. Meth. A* **329** (1993) 238
- [36] M. Regler and R. Frühwirth, “Generalization of the Gluckstern formulas. I: Higher orders, alternatives and exact results,” *Nucl. Instrum. Meth. A* **589** (2008) 109
- [37] W. B. Atwood *et al.* [Fermi-LAT], “The Large Area Telescope on the Fermi Gamma-ray Space Telescope Mission,” *Astrophys. J.* **697** (2009) 1071
- [38] K. Ozaki *et al.*, “Demonstration of polarization sensitivity of emulsion-based pair conversion telescope for cosmic gamma-ray polarimetry,” *Nucl. Instrum. Meth. A* **833** (2016) 165
- [39] D. Bernard, “MeV-GeV Polarimetry with $\gamma \rightarrow e^+e^-$: Asserting the Performance of Silicon Strip Detectors-Based Telescopes,” *Nucl. Instrum. Meth. A* **1042** (2022) 167462
- [40] W. Atwood *et al.* [Fermi-LAT], “Pass 8: Toward the Full Realization of the Fermi-LAT Scientific Potential,” 2012 Fermi Symposium proceedings - eConf C121028, [arXiv:1303.3514 [astro-ph.IM]].